Features of FeB pair light-induced dissociation and repair in silicon n^+-p-p^+ structures under ultrasound loading

O. Olikh,[1] V. Kostylyov,[2] V. Vlasiuk,[2] R. Korkishko,[2] Ya. Olikh,[2] and R. Chupryna[1]

[1]*Physics Faculty, Taras Shevchenko National University of Kyiv, Kyiv, Ukraine.*

[2]*V. Lashkaryov Institute of Semiconductor Physics of NAS of Ukraine, Kyiv, Ukraine*

(*Electronic mail: olegolikh@knu.ua)

(Dated: 21 September 2021)

The influence of ultrasound on iron–boron pair dissociation and association in silicon n^+-p-p^+ structures were investigated experimentally. The FeB pair transformations were monitored by measurements of short circuit current kinetics. It was found that ultrasound causes the decrease in both the concentration of pairs, which were dissociated by light, and time of association. The phenomenon was investigated at different light intensities, temperatures, frequencies and power of ultrasound loading. The possible mechanisms underlying the revealed effects were analysed.

I. INTRODUCTION

It is of wide knowledge that the properties of semiconducting crystals and structures are determined very much by their impurity compositions. As a result, the methods aimed at modifying the system of defects are very important for practical applications. Most of the similar methods use irradiation, thermal treatment or specific conditions of crystal growth. However, numerous experiments show that ultrasound also represents a sufficiently effective instrument in order to better control the semiconductor defects. For example, it has been found that the acoustic waves cause spatial redistribution of defects[1–6], transformation of metastable point defects[7–9], recharging of recombination centers[10,11], low temperature annealing of radiation defects[12–16]. The effects of this kind are observed in particular in silicon, which is the basic modern material used in microelectronics and solar power engineering[1,2,5,8,12,15,17,18].

The usage of active ultrasound (US) has its advantages due to local action of elastic oscillations and the possibility to adjust the external impact by changing the type, polarization or frequency of acoustic waves[19]. However, this method of modifying the defect system has not found wide application not least because of the lack of appropriate experimental research. In our opinion, it is most promising to use US loading (USL) as an additional factor of influence during various technological processes, which causes, in particular, the transformations in the defect system. This assumption is supported by the results obtained during ion implantation performed in the US field[1,17,20].

Iron is an important impurity in silicon–based integrated circuit and solar cell technology[21]. Most often, iron-related defects are the main recombination centers that determine the lifetime of minority charge carriers in particular and device characteristics in general. Therefore the methods aimed at iron gettering at various stocks have practical importance. In the publications, there is rather much information about this kind of defects. It is known that in thermal equilibrium at room temperature virtually all Fe_i is present as Fe_iB_s pairs in Si:B[22,23]. FeB pair dissociation can be accomplished by illumination at room temperature, by minority carrier injection, or by increasing the temperature[22,24,25]. Moreover, ultrasound

vibrations with the frequency of $25-80$ kHz and acoustic lattice deformation amplitude of $10^{-6}-10^{-5}$ have been found to be capable of destroying FeB pairs[26,27]. In practice, however, the most widely used technique is light-induced dissociation. The peculiarities of the dissociation and subsequent repair are well studied[22–24,28–33]. However, to the best of our knowledge, there are no reports about US impact on these processes.

Our aim is to study experimentally the influence of ultrasound loading with the frequency of $2-30$ MHz and lattice deformation $< 2 \cdot 10^{-6}$ on the processes of $FeB \leftrightarrow Fe_i + B_s$ transformations in silicon solar cells (SCs). The prethreshold intensity is used with the aim to prevent irreversible changes of the material properties. The obtained results can be used for subtle acoustically controlled tuning of the processes involved in iron atom gettering.

II. EXPERIMENTAL AND CALCULATION DETAILS

The n^+-p-p^+-Si samples used in the experiment are shown in Fig. 1. The structure was fabricated from a 380 μm thick p-type boron doped Czochralski silicon wafer with [100] orientation and resistivity of 10 Ohm·cm. The n^+ emitter with surface resistance of about $20-30$ $\Omega/\square$ and thickness of 0.7 μm was formed by phosphorus diffusion at 940°C. The anti-recombination isotype barrier was created by using p^+ layer ($10-20$ $\Omega/\square$, 0.6 μm) formed by boron diffusion at 985°C. The antireflective and passivating SiO_2 (40 nm) and Si_3N_4 (30 nm) layers were formed on the front surface as well. The solid and grid Al contacts were formed on the rear and front surfaces respectively. The samples used in the experiment had an area of 1.52×1.535 cm^2.

To dissociate FeB pairs the frontal side of the sample was illuminated with a halogen lamp with radiation intensity W_{ill} of $0.08-0.20$ W/cm^2. The illumination time t_{ill} is up to 30 s.

The FeB pair association was monitored by measurements of kinetics of short circuit current $I_{SC}(t)$ after halogen lamp illumination —- see Fig. 2. I_{SC} was measured under SC illumination by a low intensity monochromatic light source (light emitting diode SN–HPIR940nm–1W with light wavelength $\lambda = 940$ nm). LED illumination was weak (the excess density of carriers $\Delta n < 10^{12}$ cm^{-3}, the duty cycle while of $I_{SC}(t)$

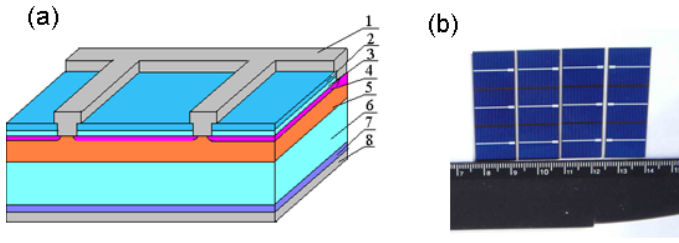FIG. 1. (a) Scheme of the sample. 1 —— frontal Al electrode; 2 —— Si$_3$N$_4$; 3 —— SiO$_2$; 4 —— induced n^{++}-layer; 5 —— diffusion n^+-layer; 6 —— p-base region; 7 —— diffusion p^+-layer; 8 —— rear Al electrode. (b) View of real solar cells; the photo was taken from the side of frontal metal electrode.
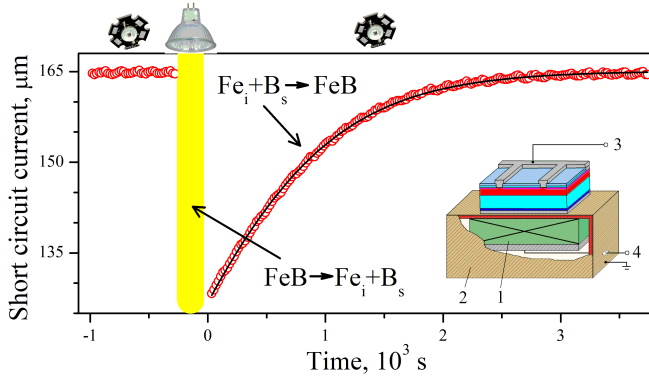

FIG. 2. Kinetics of short circuit current after intensive illumination. The marks are the experimental results, the line is the fitted curve using Eqs. (1)-(8). The zero of time corresponds to the moment of intensive illumination termination. $T = 340$ K. Inset: Scheme of USL. 1 —— piezoelectric transducer; 2 —— metal (Cu) foil , 3 and 4 — contact to I--V measure and to ultrasound excitation, respectively.

measuring was 0.5%) and did not result in FeB dissociation. After halogen lamp illumination termination, FeB pairs form again and the starting value of I_{SC} is completely recovered.

In fact, in conditions of homogeneous carrier generation in the base, which is several minority carrier diffusion lengths L_n, the short circuit current can be described as follows[34,35]:

$$I_{SC}(t) = \frac{P_{ph}(1-R_{ph})q\beta\lambda}{hc} \cdot \frac{\alpha_{ph}\sqrt{\mu_n kT\tau(t)/q}}{1+\alpha_{ph}\sqrt{\mu_n kT\tau(t)/q}}, \quad (1)$$

where $\alpha_{ph} = \alpha_{ph}(T,\lambda)$ is the coefficient of light absorption, P_{ph} is the light power, R_{ph} is the coefficient of reflection, β is the coefficient of quantum yield, μ_n is the electron mobility, τ is the minority carrier lifetime in the base. In the assumption that it is the iron related defects that play an essential role in the recombination, the following expression can be used to estimate τ:

$$\frac{1}{\tau(t)} = \frac{1}{\tau_i} + \frac{1}{\tau_{SRH}^{Fe_i}(t)} + \frac{1}{\tau_{SRH}^{FeB}(t)} + \frac{1}{\tau_{other}}, \quad (2)$$

where τ_i is the lifetime associated with intrinsic recombination, $\tau_{SRH}^{Fe_i}$ and τ_{SRH}^{FeB} are related to the recombinations at interstitial iron atoms Fe$_i$ and at FeB pairs, accordingly; τ_{other} de-

scribes further recombination channels (other impurities, lattice defects, surface recombination). In order to calculate $\tau_{SRH}^{Fe_i}$ and τ_{SRH}^{FeB}, Shockley–Read–Hall model was used

$$\tau_{SRH}^{Fe_i,FeB}(t) = \frac{\tau_{p0}^{Fe_i,FeB}(t)\cdot(n_0+n_1^{Fe_i,FeB}+\Delta n)}{N_A+n_0+\Delta n} + \frac{\tau_{n0}^{Fe_i,FeB}(t)\cdot(N_A+p_1^{Fe_i,FeB}+\Delta n)}{N_A+n_0+\Delta n}, \quad (3)$$

where N_A is the material's doping level ($1.4\cdot10^{16}$ cm^{-3}), n_0 is the equilibrium electron concentration given by the law of mass action; n_1 and p_1 are given by

$$n_1^{Fe_i,FeB} = N_C \exp\left(-\frac{E_C-E_t^{Fe_i,FeB}}{kT}\right),$$

$$p_1^{Fe_i,FeB} = N_V \exp\left(-\frac{E_t^{Fe_i,FeB}-E_V}{kT}\right), \quad (4)$$

where E_C and E_V are the energies of the conduction band and valence band edge, respectively, N_C and N_V are the densities of states in the conduction band and valence band, respectively, and E_t is the energy level of the relevant defect. The respective capture time constants of electrons and holes at the defect are given by

$$\tau_{p0}^{Fe_i,FeB}(t) = \frac{1}{N_{Fe,FeB}(t)\sigma_p^{Fe_i,FeB}v_{th}^p},$$

$$\tau_{n0}^{Fe_i,FeB}(t) = \frac{1}{N_{Fe,FeB}(t)\sigma_n^{Fe_i,FeB}v_{th}^n}, \quad (5)$$

where $N_{Fe}(t)$ and $N_{FeB}(t)$ are the concentration of Fe$_i$ and FeB, respectively, v_{th} is the thermal velocity, and σ_n and σ_p are the respective capture cross-sections of electrons and holes at the defect.

The time dependence of interstitial iron atom concentration after pair dissociation is described by the known expression from[36,37]:

$$N_{Fe}(t) = (N_{Fe,0}-N_{Fe,eq})\cdot\exp(-t/\tau_{ass})+N_{Fe,eq}, \quad (6)$$

where τ_{ass} is the characteristic time of the complex association, according to[24,28,29]

$$\tau_{ass} = \frac{5.7\cdot10^5}{N_A}T\exp\left(\frac{E_m}{kT}\right), \quad (7)$$

where E_m is the energy of Fe$_i^+$ migration; $N_{Fe,0}$ is the concentration of interstitial iron atoms formed due to illumination and $N_{Fe,eq}$ is the portion of interstitial iron atoms with $N_{Fe,0}$ that remain unpaired in equilibrium state. According to Wijaranakula[37], $N_{Fe,eq}$ depends on temperature, doping level and $N_{Fe,0}$: $N_{Fe,eq} = N_{Fe,eq}(T,N_A,N_{Fe,0})$. The estimations show that at 340 K $N_{Fe,eq} \simeq 0.1N_{Fe,0}$ for the samples under study.

In its turn, the iron–boron pair concentration N_{FeB}, which is formed in the result of partial association of $N_{Fe,0}$ can be estimated from

$$N_{FeB}(t)+N_{Fe}(t) = N_{Fe,0}. \quad (8)$$

In case the intensive illumination causes dissociation of all the pairs, $N_{\text{Fe},0}$ should be the same as the total concentration of the impurity iron in the structure $N_{\text{Fe,tot}}$. If the duration (or intensity) of illumination is not sufficient for total dissociation, $N_{\text{Fe},0} < N_{\text{Fe,tot}}$. In the latter case τ_{other} will also make contribution in the recombination of the FeB pairs that have not dissociated (with concentration $N_{\text{Fe,tot}} - N_{\text{Fe},0} - N_{\text{Fe,eq}}(T, N_A, N_{\text{Fe,tot}} - N_{\text{Fe},0})$) as well as the respective number of Fe_i (with concentration $N_{\text{Fe,eq}}(T, N_A, N_{\text{Fe,tot}} - N_{\text{Fe},0})$).

In our calculations, we took $\beta = 1$, $R_{ph} = 0.14$ (the result of calculations according to Klyui et al.[38]), $\mu_n(T, N_A)$ from Klaassen[39], υ_{th}^n and υ_{th}^p from Green[40], N_C, N_V from Couderc et al.[41], the defect parameters from Rougieux et al.[42], $\alpha_{ph}(T, \lambda)$ from data[43,44]. In calculating τ_i, band–to–band radiation recombination and Auger recombination were taken into account, and the temperature dependence of the corresponding coefficients was calculated according to Nguyen et al.[45] and Altermatt et al.[46]. We used Eqs. (1)-(8) to fit the experimental data $I_{\text{SC}}(t)$. As fitting parameters P_{ph}, τ_{other}, $N_{\text{Fe},0}$, and E_m were taken. The fittings were performed by using the metaheuristic method EBLSHADE[47].

The example of fitting results is shown in Fig. 2. In our case, the parameters determined by fitting had the following values. $P_{ph} = (3.6 \pm 0.2) \cdot 10^{-4}$ W which agrees well with the value measured by PowerMeter Rk-5720 ($3.5 \cdot 10^{-4}$ W). $\tau_{other} > 100$ s, which testifies that the contribution of other recombination pathways can be neglected. $N_{\text{Fe},0} = (1.6 \pm 0.1) \cdot 10^{13}$ cm^{-3}, which is close to the value obtained for the samples of the same series from L_n measuring before and after illumination ($0.5 \cdot 10^{13}$ cm^{-3}). Finally, $E_m = (0.655 \pm 0.001)$ eV. This value coincides with that well known[24,28,29,32] which is 0.66 eV. The coincidence of the values obtained by approximation with those obtained from other sources (first of all, E_m value) proves that the investigations of $I_{\text{SC}}(t)$ after intensive illumination can be applied in finding the parameters of iron-related defects. Moreover, the peculiarities of pair dissociation (see Sec. III A) found in this way also correspond to those reported in the previous publications, which testifies that this approach is quite appropriate. In fact, the time of I_{SC} recovering is an indicator of how large is the energy of migration, and the amplitude with which I_{SC} changes in the result of intensive illumination is associated with the concentration of iron atoms released in the process. It should be also noted that this approach is similar to the method proposed by Herlufsen et al.[48], in which actual concentrations of FeB pairs are estimated by the photoluminescence signal kinetics during pair association.

The measurements were carried out over a temperature range of 300˜340 K. The temperature was varied by a thermoelectric cooler controlled by STS-21 sensor and stabilized by computer-controlled PID loop.

In case of USL, the transverse (with frequency $f_{\text{US}} = 0.3$ MHz) or longitudinal ($2-31$ MHz) acoustic waves (AWs) were applied to the samples by using a piezoelectric transducer. The US intensities W_{US} and amplitudes of lattice deformation $\xi_{\text{US}} = \sqrt{2 W_{\text{US}} / \rho_{\text{Si}} \vartheta_{\text{US}}^3}$ ($\rho_{\text{Si}} = 2.33$ g/cm^3 is the silicon density, ϑ_{US} is the US velocity, 9850 m/s and 5840 m/s in

cases of longitudinal and transverse AWs, respectively) does not overcome 1.3 W/cm^2 and $2 \cdot 10^{-6}$, respectively. Since the focus of our research was the influence of elastic vibrations on FeB pair transformations, in order to avoid the effect of piezoelectric field, the transducer was shielded — see inset in Fig. 2.

## III. RESULTS AND DISCUSSION

A. FeB dissociation

In our investigation of light induced FeB pair dissociation processes, we illuminated the structure with a halogen lamp varying the time of illumination t_{ill} and afterwards measured the kinetics of short circuit current recovery —- see Fig. 3(a). As seen from the figure, the time of short circuit current recovery does not change while the amplitude of light induced changes depends on the time of illumination. Further approximation of the experimental curves by using the approach described in the previous section allowed us to estimate the number of pairs that dissociated in the result of illumination $N_{\text{Fe},0}$ as a function of t_{ill}. The experiments were carried out on a series of the samples at different light intensities and temperatures in conditions with and without US loading. The typical results are given in Fig. 4.

The obtained results show that as the illumination time grows the values of $N_{\text{Fe},0}$ increase gradually until reaching saturation. This is in complete correspondence with the results of the previous researches[22,24,28] that predict exponential decrease of pair concentration with the increase of illumination time. The saturation should correspond to the condition of complete pair dissociation. The experimentally obtained dependencies were approximated by using the following equation

$$N_{\text{Fe},0}(t_{\text{ill}}) = A \exp(-t_{\text{ill}} / \tau_{\text{dis}}) + N_{\text{Fe,fit}}, \qquad (9)$$

where τ_{dis} is the characteristic time of dissociation, $N_{\text{Fe,fit}}$ is the value corresponding to saturation. The examples of approximation curves are given in Fig. 4, and the values of the parameters obtained by approximation — in Fig. 5.

On the other way, the equilibrium between free Fe_i and $\text{Fe}_i B_s$ is determined by the following rate equations

$$\text{Fe}_i + \text{B}_s \xrightarrow{R_a} \text{FeB},$$
$$\text{FeB} \xrightarrow{R_d} \text{Fe}_i + \text{B}_s, \qquad (10)$$
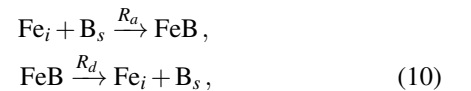
where $R_a = \tau_{\text{ass}}^{-1}$ and R_d are the association and dissociation rates of FeB pairs, respectively. From Eq. (10), taking into account that $N_{\text{Fe}} = N_{\text{Fe,tot}} - N_{\text{FeB}}$ and $N_{\text{Fe}}(t_{\text{ill}} = 0) = N_{\text{Fe,eq}}$, the time dependent interstitial iron content during illumination can be described as follows

$$N_{\text{Fe}}(t_{\text{ill}}) = \left(N_{\text{Fe,eq}} - N_{\text{Fe,tot}} \frac{R_d}{R_d + R_a} \right) \exp[-(R_d + R_a) t_{\text{ill}}] +$$
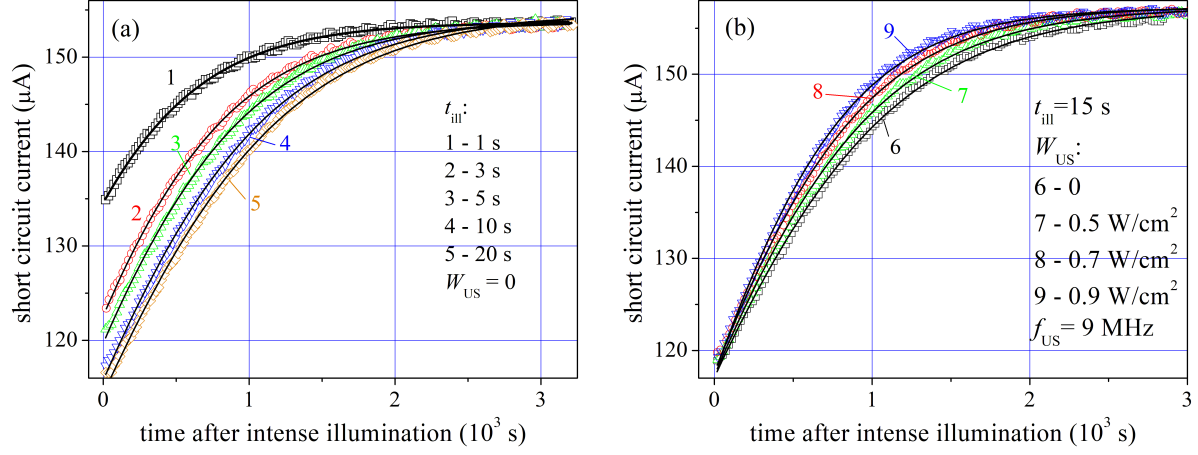$$N_{\text{Fe,tot}} \frac{R_d}{R_d + R_a}. \qquad (11)$$

FIG. 3. Typical kinetics of short circuit current after intensive illumination of different duration (a) and USL intensity (b). The marks are the experimental results, the lines are the curves fitted by using Eqs. (1)-(8). t_{ill}, s: 1 (curve 1), 3 (2), 5 (3), 10 (4), 15 (6-9), 20 (5). W_{US}, W/cm^2: 0 (1-6), 0.5 (7), 0.7 (8), 0.9 (9). $f_{US} = 9$ MHz, $T = 340$ K.
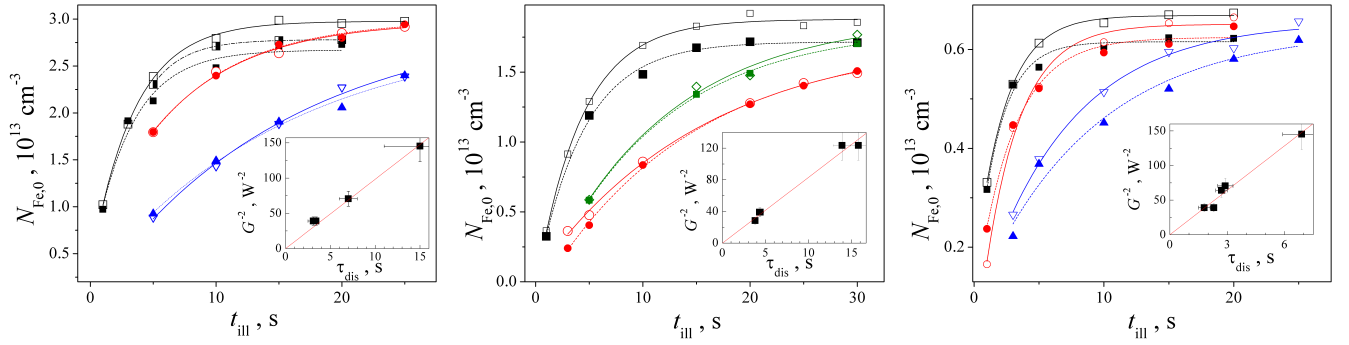

FIG. 4. Concentration dependence of interstitial atoms due to light induced dissociation on illumination time. The marks are the experimental results, the lines are the curves fitted by using Eq. (9). Empty circles and solid lines are used for the case without USL, filled circles and dashed lines — for the case of USL. W_{ill}, W/cm^2: 0.16 (curves 1-3, 8-11, 14, 15), 0.12 (4, 5, 16, 17), 0,09 (12, 13), 0.08 (6,7,18,19). W_{US}, W/cm^2: 0.9 (2, 5, 7), 0.6 (3, 9, 11, 13), 0.1 (15, 17, 19). f_{US}, MHz: 9,0 (2, 3, 5, 7), 0.3 (9, 11, 13), 5,0 (15, 17, 19); T, K: 340 (1-9,12-19), 320 (10,11). Samples SC350-1 (a), SC350-2 (b), SC349-1 (c). Insets: τ_{dis} are plotted against W_{ill}^{-2}. The lines are the curves fitted by $\tau_{dis} = const \cdot W_{ill}^{-2}$.

The comparison of Eqs. (9) and (11) shows that $\tau_{dis}^{-1} = R_a + R_d$, $N_{Fe,fit} = N_{Fe,tot} R_d / (R_a + R_d K d)$. It should be noted that in our case (see Sec. III B) $\tau_{ass} \gg \tau_{dis}$ (without USL $\tau_{ass} \simeq 700$ s at 340 K and $\tau_{ass} \simeq 13000$ s at 300 K). Therefore, $R_d \ggg R_a$ and $\tau_{dis}^{-1} \simeq R_d$, $N_{Fe,fit} \simeq N_{Fe,tot}$.

As for the case without USL, we should note the following. First, for every sample $N_{Fe,fit}$ remains constant and does not depend on illumination intensity and temperature (red and pink unhatched bars in Fig. 5). This is quite expectable if we assume that in this case $N_{Fe,fit} = N_{Fe,tot}$. Second, the value of τ_{dis} (hatched bars in Fig. 5) depends on W_{ill} and T. It is well known[22,28,49] that the dissociation rate of FeB pairs increases quadratically with increasing illumination intensity. In the insets in Fig. 4 the values of τ_{dis} are plotted against W_{ill}^{-2}. The linearity of the obtained curves is in complete coincidence with the reported data and can serve as an additional proof of the suggested approach applicability in estimating iron-related defect parameters. Moreover, it is known[50] that the dissociation time decreases approximately twice per 20°C increase. In our experiment, $\tau_{dis} = (11 \pm 4)$ s for sample SC350-2 (Figs. 4(b) and 5(b)) at $T = 320$ K, and at 340 K, it comprised 4.3 ± 0.3 s, which justifies the expectations.

Another reason why it is advisable to analyze ISC kinetics is the behavior of τ_{other} revealed in the experiments. In the case when τ_{ill} corresponds to the values of $N_{Fe,0}$ close to saturation, the other recombination channels can be neglected ($\tau_{other} > 100$ ms). In the case when the values of τ_{ill} are small, τ_{other} changes in the range $10^{-6} - 10^{-4}$ s beginning to increase as the illumination time increases. In terms of the proposed approximation, this indicates that some part of FeB pairs have not dissociated and the value of τ_{other} is related to recombination on iron-related defects that do not reconstruct when the sample is kept in darkness. In order to support this assumption the quantity τ_{other}^{calc} was estimated as follows

$$\tau_{other}^{calc} = \left(\left(\tau_{SRH}^{Fe_i} \right)^{-1} + \left(\tau_{SRH}^{FeB} \right)^{-1} \right)^{-1}$$
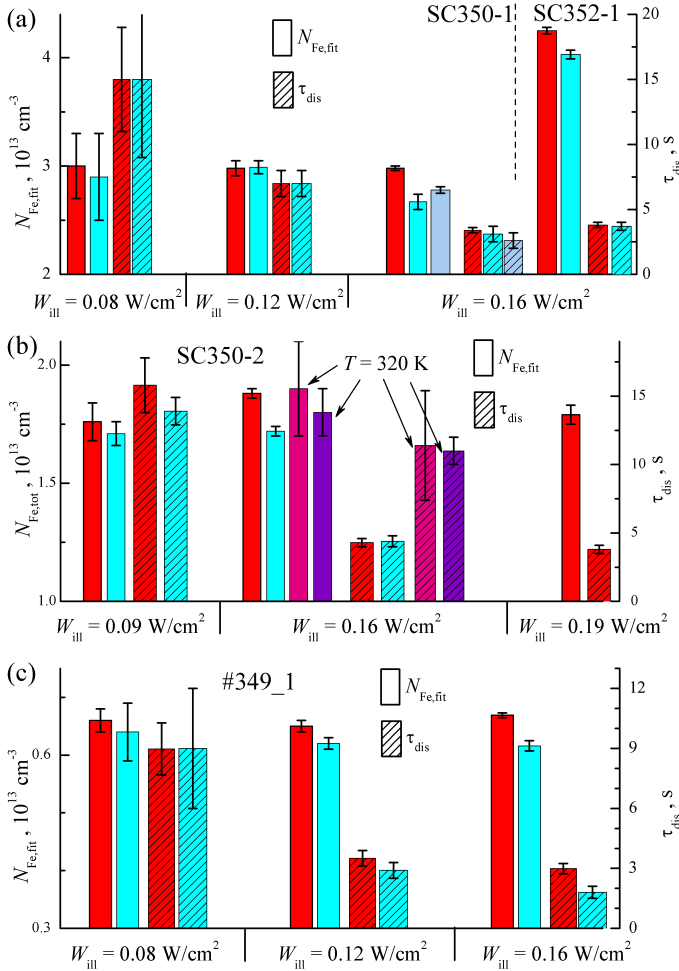
FIG. 5. The value of maximum concentrations of light released iron atoms (unhatched bars) and characteristic dissociation time (hatched bars) obtained by approximating experimental dependencies by Eq. (9). Red bars correspond to cases without USL, blue ones — with USL. Violet and pink bars (panel b) are obtained at $T = 320$ K, the rest — at $T = 340$ K. The conditions of USL for samples SC350-1, SC350-2, SC349-1 are identical with those given in the caption to Fig.3. For SC352-1 fUS = 5.9 MHz, WUS = 1.0 W/cm^2.

where $\tau_{SRH}^{Fe_i}$ and τ_{SRH}^{FeB} were calculated by Eq. (3) for defect concentrations $N_{Fe} = N_{Fe,eq}(N_{Fe,tot} - N_{Fe,0})$ and $N_{FeB} = N_{Fe,tot} - N_{Fe,0} - N_{Fe}$, accordingly. Fig. 6 compares τ_{other}^{calc} and τ_{other} obtained in the same conditions. It is well seen that their values are very similar.

Paying our attention back to the impact of acoustic waves on the processes of light induced dissociation of FeB pairs, the following should be noted. First, USL actually does not influence magnitude of τ_{dis}: in Fig. 5 the heights of neighbouring hatched red and blue bars are similar in the range of error for all the cases. Second, some pairs do not dissociate under USL: $N_{Fe,fit}(W_{US} > 0) < N_{Fe,fit}(W_{US} = 0)$. How large the portion of these pairs is, depends on US intensity (see Figs. 4(a), 5(a), $W_{ill} = 0.16$ W/cm^2); and at maximum W_{US} values this portion reaches 10%. It should be noted that this [effect] is observed only in case when light induced
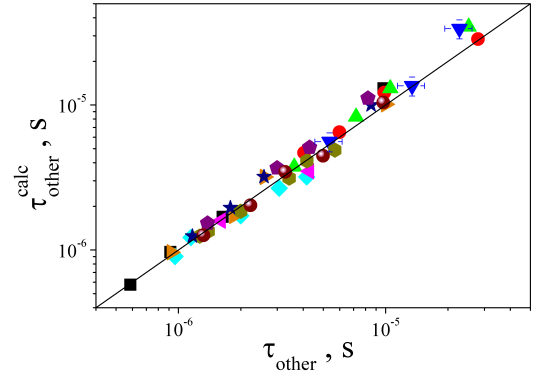

FIG. 6. τ_{other} is plotted against those calculated from $N_{Fe,0}$ and $N_{Fe,fit}$ values (see text above). Different points mark different samples and illumination conditions. The black solid line is the identify line servings as the references.

pair dissociation is close to saturation. If W_{ill} (or temperature), however, is that a part of iron atoms stays near the substitutional boron atoms at the given illumination times, then $N_{Fe,fit}(W_{US} > 0) \simeq N_{Fe,fit}(W_{US} = 0)$.

B.   FeB association

It has also been found that USL accelerates FeB pair association — see. Fig. 3(b). As seen from the figure, the main result of ultrasound excitation in the structure is the decrease in time of short circuit current recovery. Since in approximating experimental dependencies $I_{SC}(t)$ we assumed that pre exponential multiplier in Eq. (7) does not depend on USL (but relies only on the temperature and level of base doping), in order to find numerical characteristic of this effect, we used the change in migration energy ΔE_{US}, i.e. it was assumed that

$$E_m \xrightarrow{ultrasound} E_{m,0} - \Delta E_{US}, \qquad (12)$$

where $E_{m,0}$ is the migration energy estimated without USL, ΔE_{US} is the acoustically induced (AI) change in migration energy. It is seen from Fig. 3(b) that ΔE_{US} depends on acoustic wave intensity. Fig. 7 presents the dependencies $\Delta E_{US} = \Delta E_{US}(W_{US})$ at varied US frequencies and for the samples with different iron content (estimated by the dependencies similar to those given in Fig. 4) under USL. The presented data show that

1. ΔE_{US} shows practically linear dependence on US intensity;

2. Effectiveness of AI change in migration energy decreases as the US frequency increases; transverse waves, despite their low frequency, less strongly impact the processes of iron ion diffusion;

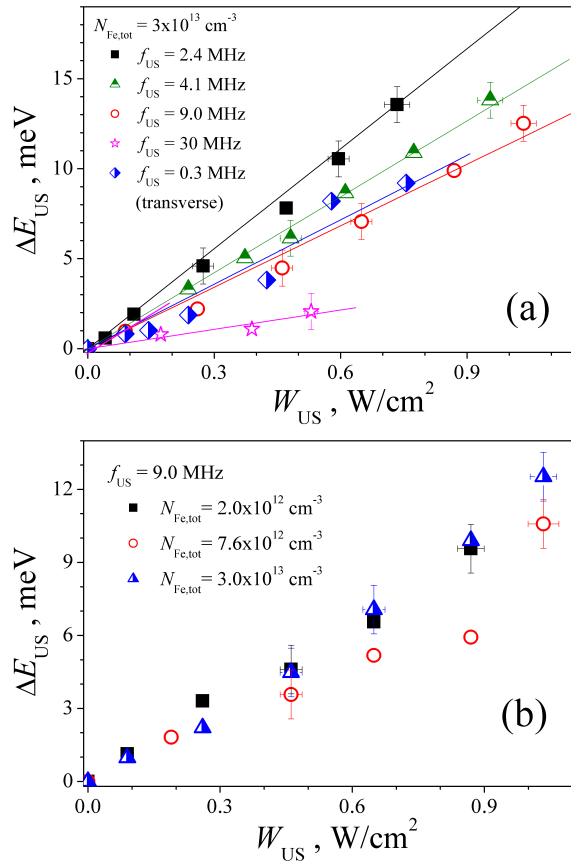3. the magnitude of AI effect practically does not depend on iron concentration;

FIG. 7. Dependencies of AI change in migration energy on US intensity for various frequencies (a) and samples with various iron concentrations (b). $T = 340$ K. The points were obtained by approximating experimental dependencies, the lines are the linear fitted curves.

4. AI change in migration energy can be as high as 13 meV.

ΔE_{US} has not been found to depend on illumination intensity.

The data presented in Fig. 7 were obtained at 340 K. With the decrease of temperature, AI effect decreases —- see Fig. **??**. As seen from the figure, temperature dependencies of ΔE_{US} are close to linear:

ACKNOWLEDGMENTS

DATA AVAILABILITY STATEMENT

The data that support the findings of this study are available from the corresponding author upon reasonable request.

[1] M. Jivanescu, A. Romanyuk, and A. Stesmans, J. Appl. Phys. **107**, 114307 (2010).
[2] A. Gorb, O. Korotchenkov, O. Olikh, A. Podolian, and R. Chupryna, Solid-State Electron. **165**, 107712 (2020).
[3] S. Ostapenko, Applied Physics A: Materials Science & Processing **69**, 225 (1999).
[4] B. Zaveryukhin, N. Zaveryukhina, and O. M. Tursunkulov, Tech. Phys. Lett. **28**, 752 (2002).
[5] N. Zaveryukhina, E. Zaveryukhina, S. Vlasov, and B. Zaveryukhin, Tech. Phys. Lett. **34**, 241 (2008).
[6] I. Dirnstorfer, W. Burkhardt, B. K. Meyer, S. Ostapenko, and F. Karg, Solid State Commun. **116**, 87 (2000).
[7] I. Buyanova, S. S. Ostapenko, A. Savchuk, and M. K. Sheinkman, in *Defects in Semiconductors 17*, Materials Science Forum, Vol. 143, edited by H. Heinrich and W. Jantsch (Trans Tech Publications, 1993) pp. 1063–1068.
[8] I. Ostrovskii, O. Korotchenkov, O. Olikh, A. Podolyan, R. Chupryna, and M. Torres-Cisneros, J. Opt. A: Pure Appl. Opt. **3**, S82 (2001).
[9] T. Wosinski, A. Makosa, and Z. Witczak, Semicond. Sci. Technol. **9**, 2047 (1994).
[10] O. Olikh, Ultrasonics **56**, 545 (2015).
[11] O. Korotchenkov and H. Grimmeiss, Phys. Rev. B **52**, 14598 (1995).
[12] A. O. Podolian, A. B. Nadtochiy, and O. A. Korotchenkov, Tech. Phys. Lett. **38**, 405 (2012).
[13] Y. Olikh, M. Tymochko, and A. Dolgolenko, Tech. Phys. Lett. **32**, 586 (2006).
[14] I. Ostrovskii, N. Ostrovskaya, O. Korotchenkov, and J. Reidy, IEEE Trans. Nucl. Sci. **52**, 3068 (2005).
[15] P. Parchinskii, S. Vlasov, and L. Ligai, Semiconductors **40**, 808 (2006).
[16] O. Konoreva, Y. M. Olikh, M. Pinkovska, O. Radkevych, V. Tartachnyk, and V. Shlapatska, Superlattices Microstruct. **102**, 88 (2017).
[17] A. Romanyuk, P. Oelhafen, R. Kurps, and V. Melnik, Appl. Phys. Lett. **90**, 013118 (2007).
[18] O. Y. Olikh, K. V. Voytenko, and R. M. Burbelo, J. Appl. Phys. **117**, 044505 (2015).
[19] O. Y. Olikh, A. M. Gorb, R. G. Chupryna, and O. V. Pristay-Fenenkov, J. Appl. Phys. **123**, 161573 (2018).
[20] A. Romanyuk, V. Spassov, and V. Melnik, J. Appl. Phys. **99**, 034314 (2006).
[21] A. A. Istratov, H. Hieslmair, and E. Weber, Appl. Phys. A **70**, 489–534 (2000).
[22] L. J. Geerligs and D. Macdonald, Appl. Phys. Lett. **85**, 5227 (2004).
[23] D. Macdonald, T. Roth, P. N. K. Deenapanray, K. Bothe, P. Pohl, and J. Schmidt, J. Appl. Phys. **98**, 083509 (2005).
[24] C. Möller, T. Bartel, F. Gibaja, and K. Lauer, J. Appl. Phys. **116**, 024503 (2014).
[25] G. Zoth and W. Bergholz, J. Appl. Phys. **67**, 6764 (1990).
[26] S. S. Ostapenko, L. , Jastrzebski, and B. Sopori, Semicond. Sci. Technol. **10**, 1494 (1995).
[27] S. S. Ostapenko, L. Jastrzebski, J. Lagowski, and B. Sopori, Appl. Phys. Lett. **65**, 1555 (1994).
[28] N. Khelifati, H. S. Laine, V. Vähänissi, H. Savin, F. Z. Bouamama, and D. Bouhafs, Phys Status Solidi A **216**, 1900253 (2019).
[29] J. Tan, D. Macdonald, F. Rougieux, and A. Cuevas, Semicond Sci. Technol. **26**, 055019 (2011).
[30] K. Lauer, C. Möller, D. Debbih, M. Auge, and D. Schulze, in *Gettering and Defect Engineering in Semiconductor Technology XVI*, Solid State Phenomena, Vol. 242 (Trans Tech Publications Ltd, 2016) pp. 230–235.
[31] X. Zhu, D. Yang, X. Yu, J. He, Y. Wu, J. Vanhellemont, and D. Que, AIP Adv. **3**, 082124 (2013).
[32] D. Macdonald, A. Cuevas, and L. J. Geerligs, Appl. Phys. Lett. **92**, 202119 (2008).
[33] T. Bartel, F. Gibaja, O. Graf, D. Gross, M. Kaes, M. Heuer, F. Kirscht, C. Möller, and K. Lauer, Appl. Phys. Lett. **103**, 202109 (2013).
[34] A. Fahrenbruch and R. Bube, *Fundamentals of Solar Cells: Photovoltaic Solar Energy Conversion* (Academic Press, 1983) p. 580.
[35] M. Razeghi and A. Rogalski, J. Appl. Phys. **79**, 7433 (1996).
[36] J. D. Murphy, K. Bothe, M. Olmo, V. V. Voronkov, and R. J. Falster, J. Appl. Phys. **110**, 053713 (2011).
[37] W. Wijaranakula, J. Electrochem. Soc. **140**, 275 (1993).

[38] N. Klyui, V. Kostylyov, A. Rozhin, V. Gorbulik, V. Litovchenko, M. Voronkin, and N. Zaika, Opto-Electr. Rev. **8**, 402 (2000).

[39] D. Klaassen, Solid-State Electron. **35**, 953 (1992).

[40] M. A. Green, J. Appl. Phys. **67**, 2944 (1990).

[41] R. Couderc, M. Amara, and M. Lemiti, J. Appl. Phys. **115**, 093705 (2014), https://doi.org/10.1063/1.4867776.

[42] F. E. Rougieux, C. Sun, and D. Macdonald, Sol. Energy Mater. Sol. Cells **187**, 263 (2018).

[43] K. Rajkanan, R. Singh, and J. Shewchun, Solid-State Electron. **22**, 793 (1979).

[44] M. A. Green and M. J. Keevers, Progress in Photovoltaics: Research and Applications **3**, 189 (1995).

[45] H. T. Nguyen, S. C. Baker-Finch, and D. Macdonald, Appl. Phys. Lett. **104**, 112105 (2014), https://doi.org/10.1063/1.4869295.

[46] P. P. Altermatt, J. Schmidt, G. Heiser, and A. G. Aberle, J. Appl. Phys. **82**, 4938 (1997), https://doi.org/10.1063/1.366360.

[47] A. W. Mohamed, A. A. Hadi, and K. M. Jambi, Swarm Evol. Comput. **50**, 100455 (2019).

[48] S. Herlufsen, D. Macdonald, K. Bothe, and J. Schmidt, physica status solidi (RRL) – Rapid Research Letters **6**, 1 (2012).

[49] J. Schmidt, K. Bothe, V. V. Voronkov, and R. Falster, physica status solidi (b) **257**, 1900167 (2020).

[50] J. Lagowski, P. Edelman, A. M. Kontkiewicz, O. Milic, W. Henley, M. Dexter, L. Jastrzebski, and A. M. Hoff, Applied Physics Letters **63**, 3043 (1993).